An *ab initio* study of the interaction between an iron atom and graphene containing a single Stone–Wales defect

2009 J. Phys.: Condens. Matter 21 485506

(http://iopscience.iop.org/0953-8984/21/48/485506)

J. Phys.: Condens. Matter **21** (2009) 485506 (7pp) doi:10.1088/0953-8984/21/48/485506

An *ab initio* study of the interaction between an iron atom and graphene containing a single Stone–Wales defect

Q E Wang[1], F H Wang[1], J X Shang[2] and Y S Zhou[1]

[1] Department of Physics, Capital Normal University, Beijing 100048, People's Republic of China
[2] School of Materials Science and Engineering, Beijing University of Aeronautics and Astronautics, Beijing 100083, People's Republic of China

E-mail: wangfuhe.cnu@gmail.com

Received 12 July 2009, in final form 27 September 2009
Published 11 November 2009
Online at stacks.iop.org/JPhysCM/21/485506

Abstract

The interaction between an iron atom and graphene containing a single Stone–Wales (SW) defect has been investigated by *ab initio* density functional calculations. The top site on the core defective bond-rotated carbon atom turns out to be the most favorable for iron atom adsorption. The local magnetic moment of the iron atom is 2.24 μ_B in this adsorbed system, and it can be interpreted by an effective Fe $3d^8 4s^0$ configuration caused by the strong interaction between the adatom and the core defective bond-rotated carbon atom. The defect minimizes the binding energy with respect to the adsorption of iron atoms on defect-free graphene and consequently makes the adsorbed systems more stable. Additionally, the adsorption of iron atoms on the defective graphene induces the adsorbed structures to be distorted evidently along the direction perpendicular to the graphene sheet. In particular, the band structures of these adsorbed systems, with some spin-polarized gap states lying between the π and π^* bands, are modulated by Fe 3d states in the vicinity of the Fermi level, and the gap between the valence band maximum and conduction band minimum is decreased to almost zero due to the interaction of Fe 3d states with C 2p states.

(Some figures in this article are in colour only in the electronic version)

1. Introduction

Graphene, a single layer of carbon atoms in a honeycomb lattice [1–3], has been focused intensively upon due to its distinctive band structure and some novel physical properties [4]. The sp^2 hybridization and unaffected p_z orbital are two primary characteristics in terms of its electronic structure leading to a unique band structure with a linear dispersion relation near the Dirac-points [5]. Because of its peculiar structural and electronic flexibility, graphene can be modified by means of chemical adsorption aimed at tailoring its electronic structure to achieve various properties.

Studies on the interplay of transition metal atoms with defect-free carbon allotropes such as nanotubes [6, 7], graphite [8, 9], and graphene [9, 10] demonstrated that the chemical adsorption of metal atoms on these carbon allotropes brings about transitions of electronic structure from being semi-metallic to metallic, semiconducting, and even magnetic semiconducting accompanied with some transformation of hybridization and binding mechanism. For all the studied systems, the most stable adsorption site for the iron atom is the hole site above the center of the hexagon [6–10]. In particular, it is interesting to note that the local magnetic moment of the Fe adatom is about 2.20 μ_B when it is adsorbed on the hole site in graphite and graphene, and the hole site inside the nanotubes. However, it is 3.90 μ_B when Fe is adsorbed on the hole site outside the nanotubes [6, 7]. These values are lower than the value 4.0 μ_B of the magnetic moment of a free iron atom. The lower of the magnetic moments can be attributed to the Fe 3d orbital Coulomb repulsion and 4s confinement effect, which leads to an electron transfer from 4s to 3d orbitals. Another reason for the restraint of the magnetic moment of the iron atom may be the curvature effect induced by the adsorption [6].

Defects in carbon allotropes were found to affect their electronic properties dramatically [11–14]. As an example, the Stone–Wales (SW) defect [15] is one of the most common defects in carbon allotropes created by rotating a C–C bond by 90° resulting in the formation of two pentagons and two heptagons around the two bond-rotated carbon atoms. The formation energy of the defect obtained by tight binding calculations is 5.55 eV and 5.80 eV in carbon nanotubes [16] and graphite [17], respectively. Using the Car–Parrinello approach Letardi *et al* [14] calculated the adsorption of atomic hydrogen on the SW defect in graphite. According to their results the most stable site is on the top of the core defective bond-rotated carbon atom. Zhou *et al* [13] studied adsorption of a series of different types of atoms (including: H, B, C, N, O, F, Si, P, Li, and Na) on the SW defect in carbon nanotubes by means of a first-principles discrete variational method. Their results demonstrated that the presence of the SW defect obviously minimizes the binding energies of the adatoms such as B, N, F, Si, Li, and Na, and it makes the adsorption more stable [13]. Additionally, investigations that focused on the role played by the SW defect in the case of adsorption of hydrogen on graphene were presented by Duplock *et al* [18]. In their work, it was found that there appears a spin-polarized gap state in the case of hydrogen adsorption on defect-free graphene. The spin polarization, however, is switched off when the SW defect is present in the graphene sheet. Furthermore, it was demonstrated that the combined effect of high curvature and the SW defect makes the adsorption of hydrogen more stable.

Due to the singularity of the SW defect, the properties of Fe adsorbed graphene containing a single SW defect are worthy of being investigated. What are the results for the adsorption of transition metal atoms on graphene containing a SW defect? In this work, the interactions between an iron atom and graphene containing a single SW defect are investigated in the framework of first-principles calculations. In section 2 we introduce the methodology we used in all calculations, and thereafter we present discussions of our calculated results. Finally, some conclusions are drawn in section 4.

2. Methodology and models

All calculations were performed with a spin-polarized projector-augmented wave (PAW) [19] approach based on the density functional theory method as implemented into the Vienna *ab initio* simulation package (VASP) code [20, 21]. The cutoff energy of the plane waves was set to 450 eV, which was found to converge the total energy of the physical models efficiently. The interaction between nuclei and electrons was described by the PAW method in which the 3d4s and 2s2p orbitals were treated as valence states for iron and carbon, respectively. The generalized gradient approximation (GGA) designed by Perdew and Wang (PW91) [22] was used for the exchange–correlation potentials. The Brillouin zone (BZ) integration was performed within the Monkhorst and Pack scheme [23], and the BZ sampling was set to $4 \times 4 \times 1$ using a Gamma centered grid for all calculations. In order to reduce the interaction of iron atoms in neighboring supercells,

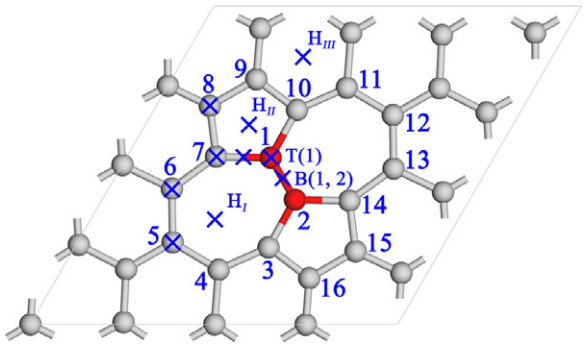

Figure 1. The supercell of graphene containing a single SW defect. For convenience, some carbon atoms are labeled with numbers. The possible adsorption sites for Fe are labeled with crosses. The top, bridge, and hole sites are labeled by T, B, and H, respectively. The two core bond-rotated carbon atoms are represented by dark (red) balls.

a 4×4 graphene supercell containing 32 carbon atoms was employed, and the separation between graphene sheets along z direction perpendicular to the sheets was set to 10 Å. The final atomic positions were obtained when no forces acting on all atoms exceeded 0.01 eV Å^{-1}. Structural optimizations were performed by the conjugate gradient method. To improve the convergence we introduced the Fermi–Dirac smearing method [24] with a broadening width of $\sigma = 0.2$ eV. The necessary convergence tests were performed before all calculations.

The possible adsorption sites for the iron atom are the top site (denoted by T) over a carbon atom, the bridge site (denoted by B) over bond between two adjacent carbon atoms, and the hole site (denoted by H) over the center of the polygons. The possible top, bridge, and hole sites on the graphene with a SW defect are shown in figure 1. In order to manifest the distortion that may be expected as an analogy with the curvature effect in nanotubes occurring in the adsorbed structures, $D_i (i = 1, 2, 3)$ [14] is introduced to represent the magnitude of distortion rate along the x, y, and z directions. D_i is calculated through the expression

$$D_i = \frac{100}{N} \sum_{j=1}^{N} (r_i^j - r_i'^j)^2 \qquad (i = 1, 2, 3) \qquad (1)$$

where N is the total number of carbon atoms, r_i represents the coordinates of the clean defective structure, and r_i' those relative to the adsorbed structure relaxed. To show the subtle difference of diverse configurations clearly, an amplification constant of 100 was employed there. The binding energies we obtained are calculated through the expression

$$E_b = E_{ad} - (E_{clean} + E_{Fe}^{atom}) \qquad (2)$$

where E_{ad} is the spin-polarized total energy for the equilibrium configuration of the absorbed structure, E_{clean} is the energy of clean graphene, and E_{Fe}^{atom} is the spin-polarized total energy of a free iron atom at its ground state.

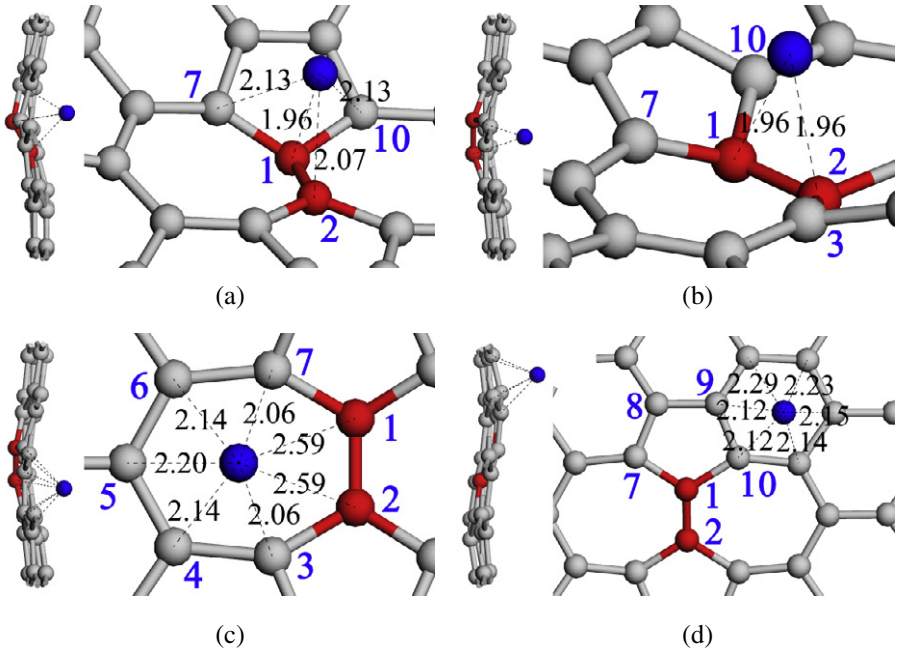

Figure 2. The local structures of the fully-relaxed adsorbed systems for (a) T(1), (b) B(1, 2), (c) H_I, and (d) H_{III}, respectively. The Fe adatom is represented by a black (blue) ball. In order to manifest the distortion along the z direction, the side-view of the whole configuration is presented on the left side of each picture. The bond lengths (in Å) of the iron atom with its carbon neighbors are shown for each configuration, respectively.

Table 1. The bond lengths and angles of the SW defect.

Bond	$C_{1,2}$	$C_{1,7}$	$C_{5,6}$	$C_{6,7}$	$C_{7,8}$	$C_{8,9}$
Length (Å)	1.30	1.46	1.43	1.46	1.36	1.43
Angle	A_{2-1-7}	A_{7-1-10}	A_{1-7-8}	A_{7-8-9}	A_{4-5-6}	A_{5-6-7}	A_{6-7-1}
Degree	121.1	117.8	98.1	113.0	121.6	125.2	142.9

3. Results and discussion

3.1. Geometry structures of clean graphene with and without the SW defect

The geometric structures of both clean graphene with and without a SW defect are calculated. The calculated bond length of perfect graphene is 1.42 Å, which is the same as the calculated result with CASTEP by Duplock *et al* [18]. The calculated bond lengths and angles within the defective region for the defective graphene are listed in table 1. The bond length l_{1-2} between the bond-rotated carbon atoms C_1 and C_2 is 1.30 Å, and the bond length l_{7-8} between C_7 and C_8 (and equivalently l_{9-10}, l_{3-16}, and l_{14-15}) is 1.36 Å. They are smaller than that of 1.42 Å in defect-free graphene. Additionally, all the other bond lengths are larger than that in defect-free graphene. As a result, the bond angles in the heptagon are larger than that of 120° in the hexagon, while those in the pentagon are smaller than 120°. The formation energy of the defect according to our calculation is 6.05 eV, which is close to the tight binding calculations of 5.55 eV in carbon nanotubes [16] and 5.80 eV in graphite [17], respectively.

3.2. Stable adsorbed structures

All the systems adsorbed with an iron atom (on top, bridge, and hole sites) on both defect-free graphene and graphene containing a single SW defect are calculated. The calculated results for the relatively more stable systems are listed in table 2. For adsorption on defect-free graphene, the most stable one is the hole site. The bond length and the local magnetic moment of Fe is 2.17 Å and 2.25 μ_B. These results are in good agreement with the previous theoretical results [7, 10]. In the case of adsorption on graphene containing a SW defect, the iron atom placed at different top, bridge, and hole sites in the defective region as the starting positions before the relaxation eventually moves from the initial sites to the more stable places. For example, the iron atom initially placed at sites of H_{II}, T(7), B(1, 7), and T(8) migrates to T(1) after relaxation, and the Fe atom at T(5) and T(6) moves to the H_I site ultimately.

After fully-relaxed geometric optimization, as shown in table 2, T(1) is the most stable configuration. This result is in agreement with calculations of atomic hydrogen adsorption on the SW defect in graphite [14] and graphene [18]. The adsorption of the iron atom changes the core rotated C–C bond angles from 121.1° to 112.6° (angle in heptagon) and 117.8° to 113.4° (angle in pentagon) with respect to the results of clean SW defect, respectively. Therefore there is a slight indication of some sp^3-like character of the bonds with the mixing of Fe 3d orbitals. The optimized structure is shown in figure 2(a). The distance of the iron atom to the nearest carbon neighbor is 1.96 Å, which is very close to the value (2.08 Å) of an iron atom interacting with perfect graphene on the top site. Furthermore, the bond lengths of the iron atom with the other

Table 2. The calculated results of binding energy E_b, the total magnetic moment M of the whole system, and the local magnetic moment m of Fe atom, as well as its contribution from Fe 4s, 4p, and 3d orbitals. The number of nearest carbon neighbors with the same Fe–C bond length is indicated in parentheses. The distortion along three directions are shown by D_x, D_y, and D_z, respectively.

	Site	E_b (eV)	Bond length (Å)	D_x	D_y	D_z	M (μ_B)	m (μ_B)	4s (μ_B)	4p (μ_B)	3d (μ_B)
Perfect graphene	H	−0.65	2.17(6)	0.00	0.00	0.01	2.62	2.25	0.02	0.04	2.19
	T	−0.21	2.08(1)	0.00	0.00	0.03	3.82	3.31	0.24	0.04	3.03
	B	−0.18	2.20(2)	0.00	0.00	0.04	3.87	3.36	0.26	0.04	3.07
Defective graphene	T(1)	−1.68	1.96(1)	0.02	0.04	8.49	2.53	2.24	0.02	0.05	2.17
	B(1, 2)	−1.54	1.96(2)	0.02	0.06	9.40	2.54	2.33	0.02	0.03	2.28
	H_I	−1.48	2.06(2)	0.04	0.02	7.39	2.52	2.31	0.03	0.04	2.24
	H_{III}	−1.33	2.12(2)	0.01	0.02	8.09	2.58	2.31	0.02	0.04	2.25

Table 3. The changes Δz (Å) of z coordinates of carbon atoms in the defective region induced by Fe adsorption. The equivalent carbon atoms in the defective region of clean graphene are labeled by $C_{l,n}$. The values of Δz (Å) for them after Fe adsorption are both shown to manifest the symmetry being broken.

	T(1)	B(1, 2)	H_I	H_{III}
C_1	−0.73, —	−0.66, —	−0.51, —	0.32, —
C_2	−0.12, —	−0.66, —	−0.51, —	−0.20, —
$C_{3,14}$	0.12, 0.12	−0.21, −0.21	−0.21, −0.25	−0.37, −0.36
$C_{15,16}$	0.47, 0.47	0.25, 0.25	0.17, 0.20	−0.55, −0.56
$C_{4,13}$	−0.04, −0.04	−0.21, −0.21	−0.20, −0.19	−0.14, −0.13
$C_{5,12}$	−0.16, −0.16	−0.21, −0.21	−0.19, −0.17	0.02, 0.03
$C_{6,11}$	−0.29, −0.29	−0.21, −0.21	−0.20, −0.19	0.19, 0.18
$C_{7,10}$	−0.46, −0.46	−0.21, −0.21	−0.21, −0.25	0.43, 0.44
$C_{8,9}$	−0.10, −0.10	−0.25, −0.25	0.20, 0.17	0.55, 0.55

three carbon atoms are 2.13 and 2.07 Å, which are very close to each other, leading to a fact that the iron atom and its three nearest carbon neighbors are in an approximately symmetrical geometric configuration.

The Fe–C bond lengths of T(1) and B(1, 2) configurations are the same, 1.96 Å, whereas the $D_z = 9.40$ of B(1, 2) is larger than that of T(1). As shown in figures 2(a) and (b), the C_2 atom submerges evidently in the case of the B(1, 2) configuration resulting in a relatively high value of D_z, so that the distance between the iron atom and the C_2 atom shifts from 2.07 to 1.96 Å. Particularly, the same value of Fe–C distance of these two structures indicates that for the B(1, 2) configuration, the iron atom is closer to the two core defective carbon atoms. In table 3, the deformation of the defective region induced by Fe adsorption is presented by Δz for different configurations. In the cases of T(1) and B(1, 2) configurations, the deformation of the defective region is symmetrical with respect to the rotated bond, in that the values of Δz for the equivalent C atoms are same. However, this kind of symmetry is broken in H_I and H_{III} configurations, as shown in figures 2(c) and (d). The bond lengths between the iron atom and its carbon neighbors are different from each other, which can be attributed to the existence of the SW defect and the curvature effect. Consequently, the symmetry of these configuration is lower than that of the H configuration in the case of adsorption on defect-free graphene.

By analyzing the binding energy of adsorption of Fe on defective and defect-free graphene, it can be found that when the iron atom is adsorbed on the sites within the defective region, the presence of the SW defect indeed minimizes the binding energy. This demonstrates that the defect promotes the adsorption of metal particles and makes the adsorbed systems more stable as found by Zhou *et al* [13]. Additionally, it can be seen from table 2 that the adsorption of Fe on graphene containing a SW defect causes distortion which occurs mainly along the z direction, whereas in the cases of adsorption on defect-free graphene, there is no obvious curvature effect. It has been reported that the increased curvature in nanotubes caused by atomic hydrogen adsorption makes the chemisorption become exothermic leading to a stronger binding [25]. What we found is in agreement with the situation of atomic hydrogen adsorption on the SW defect. These two factors, being the distortion and the SW defect, together appear to result in the most energetically favorable configurations [14, 18]. Consequently, the SW defect has an intrinsic responding mechanism to the foreign iron atom so it can be expected that the iron atom should be trapped in the core defective region, which can be a hallmark of the SW defect on graphene.

3.3. Electronic structures and magnetic properties

The calculated band structures for different configurations are shown in figures 3 and 4, respectively. For comparison, the band structure of clean defective graphene is presented in figure 3(a). Compared to the band structure of defect-free graphene at the Dirac K-point, the presence of the SW defect results in a small gap of 0.13 eV between the π and π^* band so that the defective graphene exhibits semiconducting properties. Figures 3(b) and (c) show the majority and minority spin bands of the system with the iron atom adsorbed on the T(1) site, respectively. Both the Fe 4s majority and minority spin bands are unoccupied. The small dispersion of theses bands reveals that this is a result of weak interaction between the Fe atom and graphene. All the five Fe 3d majority spin bands are occupied, while only three Fe 3d minority spin bands are occupied. Consequently, the electronic configuration of Fe is $3d^8 4s^0$, and the electronic properties of T(1) configuration is semiconducting or semi-metallic because the whole energy gap is only 0.06 eV.

As shown in figure 4, the band structures of the B(1, 2) configuration are similar to those of the T(1) configuration. Due to the existence of Fe 3d minority spin bands near the

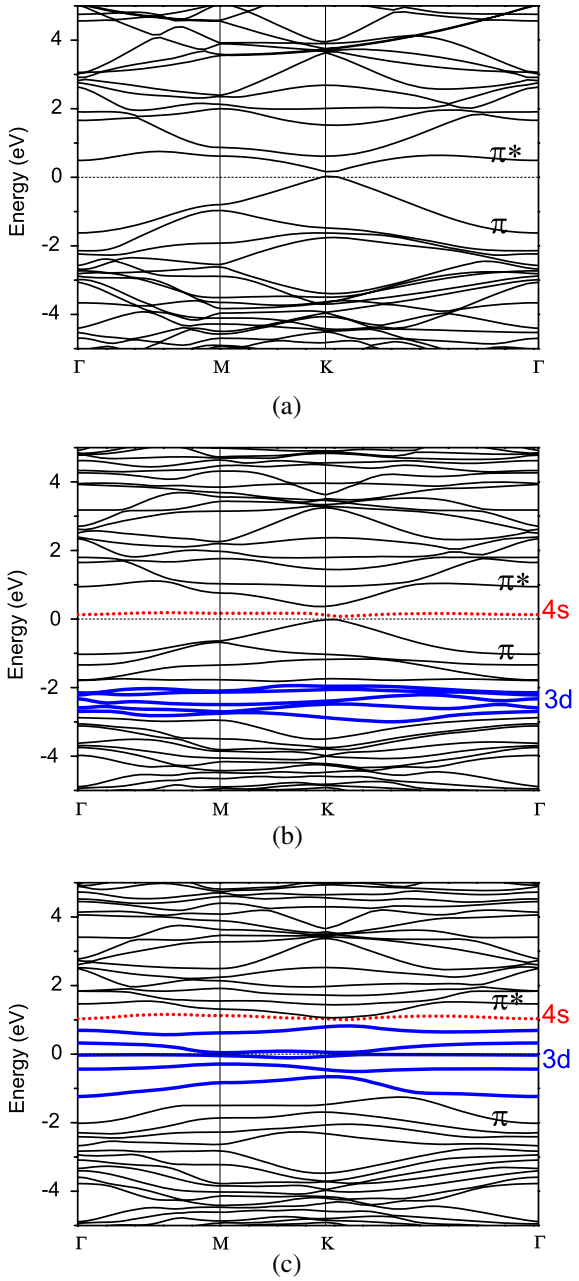

Figure 3. Band structures of the clean SW defect graphene (a), the T(1) majority spins (b), and T(1) minority spins (c). The Fermi level represented by dashed line is set to zero. The bonding and antibonding states are labeled by π and π^*. The Fe 4s and 3d states are plotted in dotted lines and thicker solid lines (red and blue), respectively.

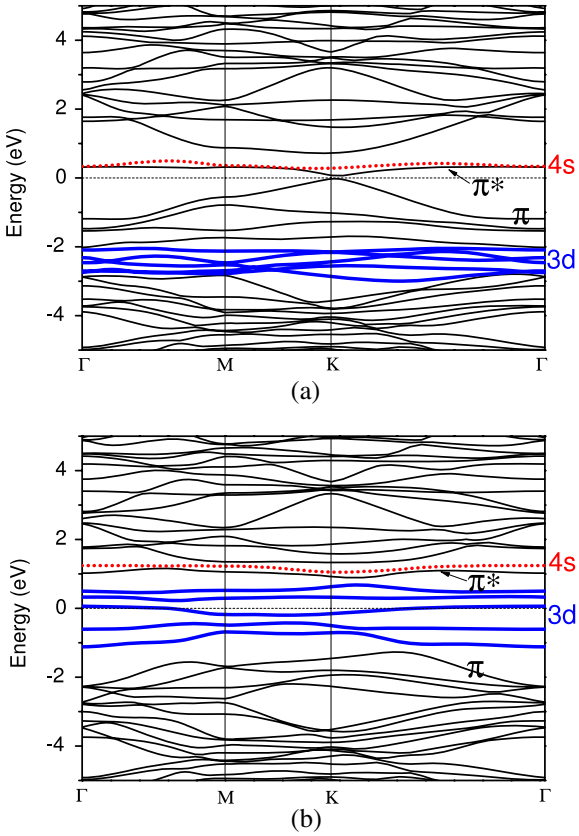

Figure 4. Band structures (a) and (b) of the system adsorbed with the iron atom on B(1, 2) site for the majority and minority spins, respectively. The Fermi level represented by dashed line is set to zero. The bonding and antibonding states are labeled by π and π^*. The Fe 4s and 3d states are plotted in dotted lines and thicker solid lines (red and blue), respectively.

Fermi level, the whole band gap is decreased to almost zero. As a result, the properties of this configuration is semi-metallic.

The magnetic properties of these adsorbed systems deserve much more attention because the role played by the defect is peculiar. Comparing the local magnetic moments of the iron atom (see table 2), it can be found that they are about 3.3 μ_B when it is adsorbed on the top or bridge sites on defect-free graphene, whereas the values of local magnetic moment of Fe are about 2.3 μ_B when it is adsorbed on the hole site on defect-free graphene or any of the sites on defective graphene, respectively. These calculated results of adsorption on defect-free graphene are in good agreement with the previous theoretical results of Fe adsorption on graphene [7] and outside the nanotubes [6, 7], and the results for the Fe adsorption on defective graphene are similar to the theoretical results for the Fe atoms adsorbed inside nanotubes [6, 7]. What is the reason for the difference in terms of the magnetic properties when the iron atom is adsorbed on different sites? One of the factors may be the intensity of the interactions between the adatom and graphene. The weaker the interaction between the iron atom and graphene is, the larger the magnetic moment is, when it is on the top or bridge site on defect-free graphene. On the contrary, when the iron atom is on the hole site on defect-free graphene or any of the sites on defective graphene the magnetic moments are small, provided that the interactions between Fe and graphene are strong. On the other hand, as discussed by Fagan *et al* [6] and Yagi *et al* [7], another factor may be the curvature effect (distortion D_z). From our calculated results, the values of magnetic moment of Fe are large when the distortions are large in the cases of defective graphene (see table 2). However, the values of the magnetic moment of Fe are large, even though the distortions are almost zero ($D_z = 0.03, 0.04$ for T and B sites, respectively), when the iron atom is adsorbed on defect-

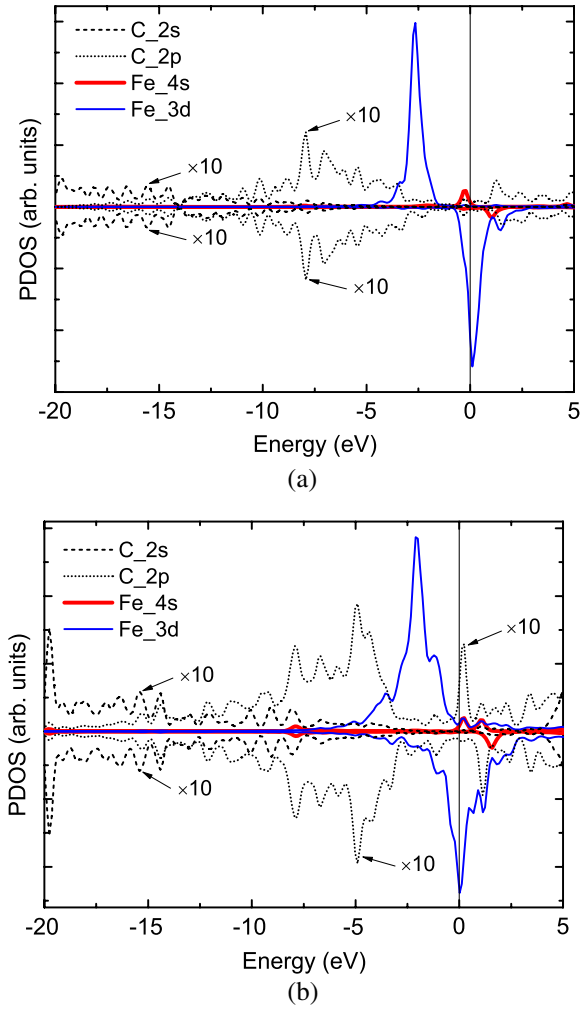

Figure 5. Projected density of states for the defect-free (a) and defective (b) systems adsorbed with the iron atom on the top site. The 2s and 2p states of the nearest carbon neighbor of Fe are magnified by 10 times. The vertical line at energy zero corresponds to the Fermi level.

free graphene. Consequently, the effect of curvature is not the determining factor.

In order to elucidate the factors affecting the magnetic properties of different adsorbed systems, the detailed density of states should be analyzed. The calculated projected density of states (PDOS) for the systems with Fe atom adsorbed on the top site on defect-free and defective graphene are shown in figures 5(a) and (b), respectively. In figure 5(a), the overlap between C 2s states and 2p states in the region of the deep energy level reveals the intrinsic nature of sp^2 hybridization of graphene. The Fe 3d up orbitals, hybridized mainly with C 2p orbitals, are totally occupied below the Fermi level, and the Fe 3d minority spins states, having a greater proportion above the Fermi level, is just partially occupied. In terms of the Fe 4s states, hybridizing with C 2p states in the vicinity of the Fermi level, the up orbitals are occupied, whereas the 4s down orbitals lying in the conduction bands are unoccupied. Consequently, it is demonstrated that when the iron atom is absorbed on defect-free graphene, an effective electronic configuration of $3d^7 4s^1$ is obtained. Comparing figures 5(b) with (a), several points about the differences of PDOS between the systems adsorbed with an iron atom on defective and defect-free graphene can be obtained. First, the sp^2 hybridization of the carbon atom in the defective system is stronger than that of the corresponding carbon atom in the defect-free system. Second, the 3d up orbitals, hybridized mainly with C 2p orbitals, are broadened, so that the interaction between Fe 3d up orbitals and C 2p orbitals is enhanced. Finally, the most significant alteration in PDOS is that the main part of the PDOS of 4s up orbitals is shifted to the region above the Fermi level, so that the number of electrons occupied in 4s orbitals is almost zero. The total effects of these alterations make the Fe adsorbed defective graphene more stable than the Fe adsorbed defect-free graphene. Consequently, there is charge transfer from Fe 4s orbitals to 3d orbitals, and an effective configuration of $3d^8 4s^0$ should be brought out with a magnetic moment of 2.24 μ_B as a result of 4s state confinement.

4. Conclusion

In conclusion, we present a systematic investigation of the properties of an iron atom interacting with the SW defect in graphene in terms of structural distortion, electronic structure, and magnetic properties. The most stable site for iron atom adsorption is the top T(1) site on one of the bond-rotated carbon atoms. The distortion and the SW defect are two factors that contribute to the strong binding of the iron atom with graphene. All the values of the local magnetic moment of the iron atom adsorbed on defective graphene are about 2.3 μ_B, which is smaller than those of Fe adsorbed on defect-free graphene. One of the key factors for the small values of the magnetic moment of Fe is the strong binding between the iron atom and its nearest carbon neighbors for different adsorbed configurations. By analyzing the band structures and PDOS, it has been demonstrated that the band gap between the valence band maximum and conduction band minimum is decreased by the interaction of Fe 3d states with C 2p states, and the electronic structures of the adsorbed systems could be semiconducting or semi-metallic. Due to the Fe intra-d Coulomb repulsion and 4s confinement effect, an effective $3d^8 4s^0$ configuration of Fe is obtained in adsorbed defective graphene. Our results could be useful for spintronics applications and could be of help in the development of magnetic nanostructures.

References

[1] Novoselov K S, Geim A K, Morozov S V, Jiang D, Zhang Y, Dubonos S V, Grigorieva I V and Firsov A A 2004 *Science* **306** 666
[2] Zhang Y, Tan Y-W, Stormer H L and Kim P 2005 *Nature* **438** 201
[3] Novoselov K S, Geim A K, Morozov S V, Jiang D, Katsnelson M I, Grigorieva I V, Dubonos S V and Firsov A A 2005 *Nature* **438** 197
[4] Geim A K and Novoselov K S 2007 *Nat. Mater.* **6** 183
[5] Beenakker C W J 2008 *Rev. Mod. Phys.* **80** 1337
[6] Fagan S B, Mota R, da Silva A J R and Fazzio A 2003 *Phys. Rev.* B **67** 205414

[7] Yagi Y, Briere T M, Sluiter M H F, Kumar V, Farajian A A and Kawazoe Y 2004 *Phys. Rev.* B **69** 075414
[8] Krüger P, Rakotomahevitra A, Parlebas J C and Demangeat C 1998 *Phys. Rev.* B **57** 5276
[9] Duffy D M and Blackman J A 1998 *Phys. Rev.* B **58** 7443
[10] Mao Y L, Yuan J M and Zhong J X 2008 *J. Phys.: Condens. Matter* **20** 115209
[11] Kaxiras E and Pandey K C 1998 *Phys. Rev. Lett.* **61** 2693
[12] Crespi V H and Cohen M L 1997 *Phys. Rev. Lett.* **79** 2093
[13] Zhou L G and Shi S Q 2003 *Carbon* **41** 613
[14] Letardi S, Celino M, Cleri F and Rosato V 2002 *Surf. Sci.* **496** 33
[15] Stone A J and Wales D J 1986 *Chem. Phys. Lett.* **128** 501
[16] Conversano R, Celino M, Cleri F, Rosato V and Volpe M 2001 *Mater. Res. Soc. Proc.* **663** A 13.4
[17] Xu C H, Fu C L and Pedraza D F 1993 *Phys. Rev.* B **48** 13273
[18] Duplock E J, Scheffler M and Lindan P J D 2004 *Phys. Rev. Lett.* **92** 225502
[19] Blöchl P E 1994 *Phys. Rev.* B **50** 17953
[20] Kresse G and Furthmüller J 1996 *Phys. Rev.* B **54** 11169
[21] Kresse G and Furthmüller J 1996 *Comput. Mater. Sci.* **6** 15
[22] Perdew J P and Wang Y 1992 *Phys. Rev.* B **45** 13244
[23] Monkhorst H J and Pack J D 1976 *Phys. Rev.* B **13** 5188
[24] Mermin N D 1965 *Phys. Rev.* **137** A 1441
[25] Gülseren O, Yildirim T and Ciraci S 2002 *Phys. Rev.* B **66** 121401